Region-specific regulation of stem cell-driven regeneration in tapeworms

Tania Rozario[1*], Edward B. Quinn[1], Jianbin Wang[2], Richard A. Davis[2], and Phillip A. Newmark[1,3,4*]

[1]Morgridge Institute for Research, Madison, WI, USA, [2]Department of Biochemistry and Molecular Genetics, RNA Bioscience Initiative, University of Colorado School of Medicine, Aurora, CO, USA, [3] Howard Hughes Medical Institute, [4]Department of Integrative Biology, University of Wisconsin-Madison, Madison, WI, USA.

* corresponding authors

Email: trozario@morgridge.org

pnewmark@morgridge.org

Abstract

Tapeworms grow at rates that rival all metazoan tissues, including during embryonic and neoplastic growth. For example, the rat intestinal tapeworm, *Hymenolepis diminuta*, produces up to 2,200 proglottids (segments), increasing in length up to 3,400 fold, and weight up to 1.8 million fold within the first 15 days of infection[1]. Tapeworms also regenerate: they shed large parts of their body, releasing their embryos to continue their life cycle, yet are able to continuously replenish proglottids and maintain an equilibrium length. Such remarkable growth and regeneration are fueled by adult somatic stem cells, which have yet to be characterized molecularly. Using *H. diminuta* as a laboratory model, we find that regeneration is limited to the tapeworm neck, making this tissue a prime source to identify stem cell genes. Using transcriptomic analyses and RNA interference (RNAi), we characterize and functionally validate the first molecular regulators of tapeworm growth and regeneration. However, we find no evidence that stem cells are restricted to the regeneration-competent neck. Instead, we find that lethally irradiated tapeworms can be rescued from death when cells from both regeneration-competent and regeneration-incompetent regions are transplanted into the neck. Furthermore, the persistence of regenerative ability over time requires signal(s) from the head, even though the head itself cannot regenerate and the head is not necessary for initial regeneration. Together, the head and neck tissue provide a microenvironment that regulates stem cells to enable region-specific regeneration in this tapeworm.

Introduction

Tapeworms are parasitic flatworms that infect humans and livestock, causing lost economic output, disease, and in rare cases, death[2]. Tapeworms are well known for their ability to reach enormous lengths. For example, humans infected with the broad or fish tapeworm, *Diphyllobothrium latum*, harbor parasites that average 6 m in length[3]. It is less commonly appreciated that tapeworms regenerate to accommodate their multi-host life cycle. Adult tapeworms in their host intestine develop proglottids that are gravid with embryos. Tapeworms pinch off the posterior and gravid sections of their body, which exit with the host excrement, to be eaten by a suitable intermediate host that supports larval tapeworm development. In spite of losing large body sections, the tapeworm does not progressively shorten; instead, it regenerates proglottids to maintain an equilibrium length. Despite this remarkable biology, tapeworms are an unexplored animal model in the study of regenerative behaviors.

Up until the 1980s, the rat intestinal tapeworm, *H. diminuta*, had been a favorite model organism among parasitologists because these parasites are easily propagated in the laboratory. A great deal of work in cell biology, biochemistry, physiology, and electron microscopy has enriched our understanding of these tapeworms[4]. With the dawn of the molecular age and the preference among scientists to concentrate on a handful of model organisms, *H. diminuta* was largely left behind.

As an obligate endoparasite, adult *H. diminuta* will expire once its host rat dies. However, the lifespan of *H. diminuta* can be uncoupled from that of its host. A single adult tapeworm can be serially amputated and transplanted into a new host intestine, where the fragment can regenerate into a mature tapeworm, even after 13 rounds of amputation over 14 years[5]. These observations

have led to speculation that *H. diminuta* may be inherently immortal, though their life span is limited by that of their host. This longevity is reminiscent of the free-living cousins of tapeworms: freshwater planarians like *Schmidtea mediterranea.* Asexual *S. mediterranea* can reproduce indefinitely by fission, and can regenerate its whole body from tiny fragments. Planarian immortality and regeneration are enabled by adult somatic stem cells called neoblasts[6-8]. These stem cells are the only dividing cells within the soma. Like planarians, *H. diminuta* maintains a population of neoblast-like adult somatic stem cells[9] that are likely responsible for their growth and regenerative ability. Recently, stem cells of other parasitic flatworms have been defined molecularly, and their maintenance depends on conserved factors such as argonaute family members and fibroblast growth factor signaling[10-12]. However, key differences also exist, as a number of conserved stem cell genes, like *piwi, vasa,* and *tudor,* are absent from the genomes of parasitic flatworms[13].

Mechanisms of stem cell regulation in parasitic flatworms are still largely unexplored, though stem cells are crucial for parasite biology and even disease. For example, the tapeworm *Echinococcus multilocularis* causes alveolar echinococcosis, in which larvae use their stem cells to grow as infiltrative cysts that can cause organ failure, and like a malignant tumor, can metastasize to secondary organs[14]. A better understanding of stem cell regulation in parasitic flatworms is needed to elucidate parasite biology and potentially, for gaining therapeutic insights.

In this study, we use *H. diminuta* to investigate the molecular basis of tapeworm regeneration. We established and refined experimental tools such as transcriptomics, *in vitro* parasite culture, RNA *in situ* hybridization, cycling cell tracing with thymidine analogs, and RNA interference (RNAi), all reported in this work. We determine that the ability to regenerate is regionally limited to the neck of adult *H. diminuta*. However, regeneration from the neck is finite

80 without signals from the tapeworm head. Using RNA sequencing (RNA-seq), we identify and
81 characterize various markers of the somatic cycling cell population, which includes tapeworm stem
82 cells. We functionally validate essential regulators of growth and regeneration. Intriguingly, our
83 analyses failed to uncover a neck-specific stem cell population that explains the regional
84 regenerative ability displayed by *H. diminuta.* Instead, we demonstrate that tapeworm regeneration
85 can be rescued by cells that are sourced from outside the neck, regardless of source-tissue
86 regeneration competence. Thus, extrinsic signals present in the tapeworm neck confer region-
87 specific regenerative ability in this tapeworm.

Results and Discussion

To examine the regeneration competence of *H. diminuta*, we amputated different anatomical fragments cut from the adult and assayed their ability to regenerate. The body plan of adult *H. diminuta* consists of a head with four suckers, an unsegmented neck (~2.5-3 mm in 6-day old worms), and a body with thousands of proglottids that grow and mature in an anterior-to-posterior direction (Fig. 1a). Previous work showed that amputated *H. diminuta* anterior fragments transplanted into rat intestines were able to regenerate into mature tapeworms[5,15]. However, using transplantation, a complete study of regeneration competence was not possible: only anterior fragments could be tested because the suckers are required to anchor the worms to the intestine. To ascertain which anatomical regions of *H. diminuta* are competent to regenerate, amputated fragments must be grown *in vitro*. We successfully established *H. diminuta in vitro* culture modified from the Schiller method[16], and tested the regeneration competence of several different 1 cm fragments (Fig. 1b-c). The anterior-most fragments (head + neck + body) were competent to regenerate, confirming previous observations using amputation and transplantation[5,15]. Additionally, anterior fragments that were first decapitated (neck + body) were also competent to regenerate proglottids. In contrast, "body only" fragments that did not contain the neck tissue were not competent to regenerate proglottids. All amputated fragments could grow in length (Fig. 1d), differentiate mature reproductive structures, and mate. However, the neck is necessary for regeneration of new proglottids over time. In no case did we observe head regeneration. Also, amputated heads alone could not regenerate proglottids *in vitro* (data not shown) nor *in vivo*[15]. To test if the neck is sufficient for proglottid regeneration, we amputated 2 mm fragments of the neck tissue and grew the fragments *in vitro*. "Neck only" fragments regenerated an average of 383

proglottids (SD=138, n=20) after 12 days *in vitro* (Fig. 1e). Thus, the tapeworm neck is both necessary and sufficient for proglottid regeneration.

Previous studies have shown that *H. diminuta* can regenerate after serial rounds of amputation and transplantation for over a decade[5] and perhaps indefinitely. Using *in vitro* culture, we confirmed that anterior fragments of *H. diminuta* can regenerate proglottids after four rounds of serial amputation followed by 12-15 days of *in vitro* culture (Fig. 1f-g) without any observable cessation of regenerative ability. Decapitated fragments were competent to regenerate proglottids after the first amputation; however, re-amputation abrogated regeneration (Fig. 1f-g). After decapitation, a definitive neck tissue could not be maintained and eventually, the whole tissue was comprised of proglottids (Fig. S1). Without the head, proglottid regeneration from the neck is finite. Thus, the tapeworm head is necessary for persistent proglottid regeneration and to maintain an unsegmented neck.

If signals from the head regulate regeneration, is regenerative potential asymmetric across the anterior-posterior (A-P) axis of the neck? We subdivided the neck into three 1 mm fragments and assayed the number of proglottids regenerated *in vitro* (Fig. 1h-i). We found that the most anterior neck fragments regenerated more proglottids than the middle or posterior neck fragments (Fig. 1h-i). Thus, only the neck is competent to regenerate proglottids, but signals from the head also regulate regeneration, resulting in an anterior bias in regenerative potential.

Why is the neck the only region competent to regenerate? One hypothesis is that pluripotent stem cells are confined to the neck. There are currently no specific molecular markers for adult tapeworm stem cells. However, like in other flatworms, the only proliferative somatic cells in *H. diminuta* are undifferentiated[17,18]. Thus, cycling somatic cells include tapeworm stem cells and any dividing progeny. To label cycling somatic cells, we used two methods: uptake of the

thymidine analog F-ara-EdU to mark cells in S-phase and fluorescent RNA *in situ* hybridization (FISH) against conserved cell cycle-regulated transcripts such as the replication licensing factor *minichromosome maintenance complex component 2* (*mcm2*) and *histone h2b* (*h2b*). Both *h2b* and *mcm2* are conserved cycling cell markers expressed in stem cells of free-living and parasitic flatworms[10,19]. We detected cycling somatic cells throughout the tapeworm body (Fig. S2a-c). Contrary to previous results[17], we also detected cycling cells in the head, though in small numbers. The scarcity of these cycling cells may be the reason they were originally missed. Taken together, cycling cells are present in tissues that are competent or incompetent to regenerate proglottids.

Though cycling cells are widely distributed, it is possible that within this population, there are stem cells of varying potency and that a pluripotent subpopulation may be restricted to the neck. To identify potential stem cell markers, we characterized the cycling cell population at the molecular level. Previously, stem cell genes had been identified in flatworms using irradiation to deplete cycling cells followed by transcriptome analysis to identify downregulated transcripts[10,19,20]. In *H. diminuta*, cycling cells are undetectable after exposure to 200 Gy irradiation (Fig. S2d). Consequently, growth and regeneration were also stunted following irradiation (Fig. 2a-b). We leveraged the sensitivity of *H. diminuta* to irradiation to identify new molecular markers of cycling somatic cells, including stem cells. Untreated and irradiated worms were cultured *in vitro* for 3 days, after which the necks were amputated and processed for RNA-seq (Fig. 2c). We assembled a *de novo* transcriptome for *H. diminuta* consisting of 14,346 transcripts (refer to methods) to which sequencing reads were mapped. Using differential gene expression analysis, we identified 683 irradiation-sensitive transcripts (downregulated; FDR $\leq$0.05) (Supplemental Table 1), cloned 335 genes, and examined their expression patterns using whole-mount colorimetric *in situ* hybridization (WISH). Using WISH, we observed that expression of

157 irradiation-sensitive genes was indeed reduced after exposure to irradiation, validating our RNA-
158 seq approach (Fig. S3).

159 In tapeworms, the position of cycling cells in the neck is spatially restricted in a pattern
160 that is conserved in multiple tapeworm species[21] (Fig. 2d-e). Cycling cells are located in the neck
161 parenchyma, which is bounded by the nerve cords. Cycling cells are not found at the animal edge
162 where differentiated cells of the muscle and tegument (parasite skin) are located[17]. This pattern
163 allowed us to use WISH to identify potential cycling cell genes. After excluding genes with
164 ubiquitous expression or poor signal by WISH, we examined gene expression for 194 irradiation-
165 sensitive genes. 62% of genes examined were expressed in the neck parenchyma, though in a
166 variety of patterns (Fig. S4a). 13% of genes examined were predominantly expressed in the neck
167 parenchyma, similar to *h2b* and *mcm2* (Fig. 2f, S4b). These include the nucleic acid binding factor
168 *Zn finger MYM type 3* (*zmym3)*, the transcription factor *suppressor of hairy wing* (*su(Hw)*), nuclear
169 lamina component *laminB receptor* (*lbr*), and *leucine-rich WD-containing gene* (*lrwd*). 25% of
170 irradiation-sensitive genes, were expressed in a minority of cells in the neck parenchyma (Fig.
171 S4c). 24% were expressed broadly, including within the neck parenchyma and at the animal edge
172 where non-cycling differentiated cells are located (Fig. S4d). In conclusion, irradiation-sensitive
173 genes identified by RNA-seq likely represent markers for stem cells, progenitors, and even
174 differentiated cells that were lost or compromised following irradiation.

175 To ascertain whether genes that showed expression in the neck parenchyma were indeed
176 expressed in cycling cells, we performed double fluorescent *in situ* hybridization (dFISH) with
177 candidate genes and either *h2b* or *mcm2*. We use *h2b* and *mcm2* interchangeably as they
178 completely co-localize in the neck parenchyma (Fig. S5). Irradiation-sensitive genes from Fig. 2f
179 were indeed expressed in cycling somatic cells (Fig. 2g-h, S6a-b). One gene, the homeobox factor,

prospero (*pros*), was expressed exclusively in a subset of cycling cells (Fig. 2i). We confirmed that irradiation-sensitive genes that only partially overlapped in the neck parenchyma, such as the Zn finger-containing genes *HDt_10981* and *HDt_05316* were expressed in a subset of cycling cells as well as non-cycling differentiated cells (Fig. S6c-d). We propose that these genes represent lineage-committed stem cells or progenitors for tissues such as muscle, neurons, tegument, or protonephridia. In summary, we performed dFISH for 53 candidates and found that 72% of genes tested were co-expressed in cycling cells (Fig. S6e, Supplemental Table 2). Our analysis revealed that there is a heterogeneous and complex mixture of cell types or states within the cycling cell population.

We reasoned that genes expressed in the majority of cycling cells would likely be essential for tapeworm growth and may regulate stem cell populations that are necessary for regeneration. Thus, we developed an RNAi protocol that allowed us to functionally investigate how candidate genes affect tapeworm growth and regeneration (Fig. 3a). As a proof of principle, we used RNAi to knock down *h2b.* Stem cells are constantly dividing and require new histone synthesis to maintain the population. Thus, downregulating expression of *h2b* in tapeworms would likely compromise growth as a result of cycling cell loss, as is the case in other flatworms[19,22]. In our RNAi paradigm, knockdown of *h2b* induced gross growth defects (Fig. 3b-c). The number of proglottids regenerated was also reduced; however, this was difficult to quantify as many RNAi worms were so thin and frail that proglottid definition was lost. We then tested two newly identified cycling cell genes: *zmym3,* and *su(Hw)* for potential roles in tapeworm growth and regeneration. Similar to knockdown of *h2b, zmym3(RNAi)* and *su(Hw)(RNAi)* each resulted in abrogated growth and regeneration. RNAi-mediated knockdown has been demonstrated in other tapeworm species[23-26], though not in *H. diminuta.* RNAi has not been widely adopted for studying

tapeworm biology due to technical challenges, like poor knockdown efficacy, inefficient penetrance, and the difficulty of *in vitro* culture. Our RNAi scheme is relatively straightforward and robust, and shows that gene inhibition can be used to uncover regulators of adult tapeworm growth and regeneration.

Are the growth defects we observe the consequence of defects in the cycling cell population? After RNAi, we quantified the number of cycling cells present by detecting F-ara-EdU^{+} cells following 1-hour exposure to the thymidine analog. Knockdown of *h2b, zmym3,* and *su(Hw)* severely reduced the number of cycling cells detectable in the neck (Fig. 3d-e). Thus, *h2b, zmym3,* and *su(Hw)* are necessary for the function of cycling cells.

The mechanism of action by *zmym3* and *su(Hw)* in *H. diminuta* is currently unknown. In mice and humans, *zmym3* acts as a transcriptional repressor with chromatin-binding properties and has been shown to regulate cell cycle progression[27] and DNA repair[28]. In *Drosophila*, *su(Hw)* binds to *gypsy* insulator sequences to regulate chromatin silencing[29]. Similar functions for these genes may be conserved in tapeworms as cell cycle regulation, DNA repair, and silencing are likely important for the regulation of tapeworm stem cells.

We have now described molecular heterogeneity within the cycling cells of the neck parenchyma and identified *h2b, zmym3,* and *su(Hw)* as functionally important in cycling cell regulation. At this point, we have not yet determined why regeneration competence is restricted to the neck. Are subsets of cycling cells distributed in a polarized manner? No gene expression pattern examined was exclusive to cycling cells of the neck. By WISH, all cycling cell genes were expressed throughout the whole tapeworm body, including *zmym3* and *su(Hw)* (Fig. 4a). Since we observed an anterior bias in regenerative ability (Fig. 1h-i), we hypothesized that stem cells may be asymmetrically distributed in the neck and detectable by RNA-seq. We performed RNA-seq of

1 mm anterior, middle, and posterior neck fragments (Fig. 1h) and identified 454 anterior-enriched and 238 anterior-depleted transcripts (Fold change ≥1.5 or ≤-1.5 respectively; FDR ≤0.05) and overlaid them with our irradiation-sensitive dataset. The majority of anterior-enriched transcripts (88%) were not irradiation sensitive (Fig. S7a). Instead, we observed that anterior-enriched and anterior-depleted genes were often expressed in corresponding gradients (Fig. 4b) but these patterns were not within the neck parenchyma. Our results suggest that the polarized signals across the neck tissue are predominantly within the non-cycling compartments.

Since our RNA-seq analysis identified transcripts that were anterior-enriched and irradiation-sensitive (Fig. S7a), we examined their expression patterns to ascertain if these genes are expressed within stem cells. We found 15 genes that are expressed in a subset of cells within the neck parenchyma, including *pros*, *solute carrier family 13* (*slc13*), *hepatocyte nuclear factor 4* (*hnf4*), and several novel genes (Fig. S7b). However, by dFISH with *mcm2*, 7/8 genes tested were not expressed in cycling cells (Fig. S7c). Only one gene, *pros,* was co-expressed in cycling cells (Fig. 2i). Our analyses have not revealed an anteriorly biased subpopulation of stem cells that confer regenerative ability. This may be due to the coarse resolution of our analysis. A more thorough characterization of tapeworm cycling cells by single-cell RNA-seq is warranted. Nonetheless, the variety of cycling cell markers we have described in this work will aid in future classification of tapeworm stem cells.

So far, we have not found evidence for a unique neck-specific subpopulation of cycling cells. This led us to hypothesize that stem cells may be distributed throughout the tapeworm, but that extrinsic signals operating in the neck are necessary to instruct stem cell behavior and/or proglottid regeneration. To pursue this hypothesis, we designed a functional assay to test populations of cells for the ability to rescue regeneration. We exposed tapeworms to a lethal dose

of irradiation, injected wild-type cells into the neck region, amputated 5 mm anterior fragments, and looked for rescue of viability and regeneration after 30 days *in vitro*. Remarkably, bulk-cell transplants were able to rescue irradiated worms that were destined to die (Fig. 4c; 44% rescue (n=41)). In no case did we observe rescue of viability or regeneration in irradiated worms that were not injected with cells or mock-injected (n=34). With this functional assay in hand, we compared cells from tapeworm anteriors (including the regeneration-competent neck) to cells from tapeworm posteriors (which are regeneration incompetent) for rescue ability. We found that cells from both regeneration-competent and regeneration-incompetent regions of *H. diminuta* were able to recue viability and regeneration in lethally irradiated tapeworms (Fig. 4d; 11% rescue for both A and P (n=37 and 35, respectively)). These results confirm that the regeneration competence of the neck tissue is not due exclusively to intrinsic properties of stem cells in this region, but to extrinsic signals that regulate competence to regenerate.

Our results suggest that in tapeworms, location matters enormously: the head and neck environment provide cues that regulate the ability of stem cells to mediate proglottid regeneration. We show that the head plays instructive roles that regulate how proglottids form and regenerate. Signals from the head may create gradients across the neck that inhibit proglottidization and are necessary to maintain the neck as an unsegmented tissue. Proglottids can only form once the inhibitory signals are sufficiently diminished (Fig. 4e). How the head regulates stem cells is less clear. The head may serve as a niche (directly or indirectly) that is necessary for the maintenance of stem cells in the neck (Fig. 4e). In this model, stem cells are collectively pluripotent only when they receive head-derived niche signals, thus limiting regenerative potential to the neck. Alternatively, stem cells may depend on a local niche that is independent of the head (Fig. 4e). In this model, stem cells have the capacity to form all cell lineages from any amputated fragment,

however, the extrinsic signals that activate proglottid formation are only found in the neck. The interplay between intrinsic and extrinsic stem cell regulatory signals has already been shown to play important roles in regeneration. Head regeneration was induced in three planarian species that were naturally regeneration deficient by manipulating the gradient of wnt signaling by RNAi[30-32]. These planarians maintained pluripotent stem cells but could not regenerate heads because of inhibitory cues from the surrounding tissue. In tapeworms, gradients of wnt signaling that delineate A-P polarity are conserved with planarians[33]. RNA-sequencing of the neck A-P axis in *H. diminuta* has revealed genes that are expressed in gradients across the neck, which could help us understand how stem cells and regeneration depend on these extrinsic signals.

Materials and Methods

Animal care and use

Infective *H. diminuta* cysts were obtained from Carolina Biologicals (132232). To obtain adult tapeworms, 100-300 cysts were fed to Sprague-Dawley rats by oral gavage in ~0.5 mL of 0.85% NaCl. Rats were euthanized in a CO_2 chamber typically 6 days post-gavage and tapeworms were flushed out of the small intestine and washed in 1X Hanks Balanced Salt Solution (HBSS; Corning) (140 mg/L $CaCl_2$, 100 mg/L $MgCl_2.6H_2O$, 100 mg/L $MgSO_4.7H_2O$, 400 mg/L KCl, 60 mg/L KH_2PO_4, 350 mg/L $NaHCO_3$, 8 g/L NaCl, 48 mg/L Na_2HPO_4, 1 g/L D-glucose, no phenol red). Rodent care was in accordance with IACUC policies and protocols.

In vitro parasite culture

Biphasic parasite cultures were prepared based on the Schiller method[16]. Briefly, the solid phase was made in 50 mL Erlenmeyer flasks by mixing 30% heat-inactivated defibrinated sheep blood (Hemostat) with 70% agar base for 10 mL blood-agar mixture per flask. Fresh blood was heat-inactivated at 56°C for 30 min then kept at 4°C and used repeatedly for one week by first warming the blood to 37°C. The agar base was prepared from 8 g Difco nutrient agar and 1.75 g NaCl in 350 mL water, autoclaved, and stored at 4°C. Before use, the agar base was microwaved to liquify, and cooled to below 56°C before mixing with warmed blood. After the blood-agar mixture solidified, 10 mL of Working Hanks 4 (WH4; 1X HBSS/4 g/L total glucose/1X antibiotic-antimycotic (Sigma)) was added. Each flask was topped with a gas-permeable stopper (Jaece Identi-plug) and pre-incubated at 37°C in hypoxia (3% CO_2/5% O_2/95% N_2) overnight before use. Before tapeworms were transferred into the flasks, the liquid phase was adjusted to pH7.5 with

200 µL 7.5% $NaHCO_3$ (Corning). Tapeworms were first washed in WH4 for 10 mins at 37°C in petri dishes pre-coated with 0.5% BSA to inhibit sticking. Transfers to pre-cultured flasks were performed by gently lifting the worms with a stainless-steel hook (Moody Tools) and immersing them in the liquid phase. Tapeworms were transferred to fresh cultures every 3 days.

Fixation and Staining

Tapeworms were heat-killed by swirling in 75-80°C water for a few seconds until the worms relaxed and elongated, then fixative (4% formaldehyde/10% DMSO/1% NP40 in Phosphate Buffered Saline with 0.3% TritonX-100 (PBSTx)) was added immediately. Tapeworms were fixed for 30 min-2hr at room temperature or overnight at 4°C. For DAPI staining, samples were incubated in 1 µg/mL DAPI (Sigma) in PBSTx overnight at 4°C. Stained tapeworms were cleared in 80% glycerol/10 mM Tris pH7.5/1 mM EDTA overnight at room temperature before mounting.

Thymidine analog uptake and staining

For BrdU pulse, tapeworms were incubated in 10 µM BrdU (Sigma) in 1% DMSO at 37°C in WH4 and processed for staining by an adapted protocol previously used on planarians[34] and schistosomes[10]. Tapeworms were killed in cold 2% HCl for 2 min with shaking every 30 seconds, fixed in cold methacarn (6:3:1 methanol:chloroform:glacial acetic acid) for 30 min at 4°C. Denaturation was performed in 2N HCl for 45 min. Blocking and antibody incubation were performed in K-block (5% Horse serum/0.45% fish gelatin/0.3% Triton-X/0.05% Tween-20/PBS) [35], before detection with anti-BrdU antibody (1:500, B35128, Invitrogen) and anti-mouse-HRP

326 secondary antibody (1:1000; Jackson). Tyramide signal amplification (TSA) reaction[36] was also
327 used.

328 For F-ara-EdU pulse, tapeworms were incubated in 0.1 μM F-ara-EdU (Sigma) in 1%
329 DMSO for 1 hr at 37°C in WH4. Tapeworms were heat-killed, fixed in 4% formaldehyde/10%
330 DMSO/1% NP40/PBSTx, permeabilized by treatment with 10 μg/mL Proteinase-K/0.1%
331 SDS/PBSTx for 10-30 min at room temperature, fixed in 4% formaldehyde/PBSTx for 10 min
332 before samples were cut into small pieces or retained whole in PBSTx. Samples were
333 permeabilized in PBSTx/10% DMSO/1% NP40 for 20min-1 hr (depending on size) before
334 performing the click-it reaction[37] with Oregon Green 488 Tyramide (Invitrogen). Signal was
335 detected using anti-Oregon Green 488-HRP antibody (1:1000; A-21253 Invitrogen) in K-block
336 followed by TSA reaction. For F-ara-EdU quantification, tiled confocal z-stacks through the
337 anterior of the worms were taken and cell numbers were counted using background subtraction on
338 Imaris.

339

340 Irradiation

341 Irradiation was performed using a CellRad irradiator (Faxitron Bioptics) at 200 Gy (150
342 kV, 5 mA). Tapeworms were irradiated in WH4 in BSA-coated petri dishes. At this dosage,
343 tapeworms degenerated and were inviable after 30 days in culture.

344

345 Transcriptome assembly

346 To construct a transcriptome for *H. diminuta,* we collected RNA from five regions: 1) head
347 and neck, 2) immature proglottids, 3) mature reproductive proglottids, 4) gravid proglottids, and
348 5) mixed larval stages isolated from beetles. The first three regions covered the entirety of 3.5-

week old adult tapeworms. The gravid proglottids were taken from the posteriors of 10-week old tapeworms. Paired-end libraries were constructed with 2 x 150 bp reads from a HiSeq2500 chip. 2 x ~30 million reads were obtained for each sample. The transcriptome was assembled from three components: 1) map-based assembly, 2) *de novo* assembly, and 3) Maker predictions from Wormbase Parasite. The map-based assembly was performed using TopHat2 with the 2014 *H. diminuta* draft genome courtesy of Matt Berriman at the Wellcome Sanger Institute. 15,859 transcripts were assembled using TopHat. *De novo* assembly was performed using Velvet/Oases and resulted in 144,682 transcripts. For the Maker predictions, there were 11,275 predicted transcripts and 73.2% matched (>95% along the length) to the TopHat transcripts. The remaining predicted transcripts that were not represented in the TopHat dataset were added to make a combined TopHat/predicted set of 17,651 transcripts. Most of the Oases transcripts matched to the TopHat/predicted set but 35,300 or 24.4% of the Oases transcripts did not (>75% match cut-off). These transcripts could be transcripts missed in the genome, transcription noise, non-coding transcripts, or contamination. We found significant contamination from beetle tissue in the larval tapeworm sample (more below). Initial filtering for contamination excluded 1,388 transcripts (from beetle, rat, bacterial, and viral sources). At this point 51,563 transcripts were retained from the three methodologies described above and were processed for further filtering.

We first filtered out additional contamination from beetle tissues. We expect that this was a large problem because during dissections, beetle tissues adhered to the tapeworm larvae and were not easily washed away. These transcripts had best hits to beetle proteins (from *Ixodes scapularis, Harpegnathos saltator, Monodelphis domestica, Nasonia vitripennis, Pediculus humanus corporis, Solenopsis invicta, Tenebrio molitor,* and *Tribolium castaneum*). Most of the transcripts were from the Oases *de novo* assembly and did not match the *H. diminuta* genome. Furthermore,

they were strongly over-represented in the larval sample only. Thus, an additional contamination filtering step was taken: transcripts from the Oases assembly without matches to the *H. diminuta* genome that showed >90% expression (by RPKM) in the larval sample were filtered out as potential contaminants. 11,918 transcripts were filtered out in this step.

To the remaining 39,645 transcripts, we applied additional filters: 1) Remove transcripts if average RPKM<1 unless the transcript is long (>1000 bp), has a long ORF (>500 bp) or is annotated. 11,615 transcripts were removed as they met none of these criteria. 2) A stringent expression cut-off was applied to the remaining Oases transcripts; transcripts were discarded if average RPKM<5 and maximum RPKM<10 unless the transcripts were long (>1000 bp), had long ORFs (>500 bp) or were annotated. 8,027 transcripts were removed. 3) 51 transcripts were removed because they are mitochondrial or rRNAs. 4) An ORF size filter was applied to remove all transcripts with ORF <300 bp unless they are annotated. 5,331 transcripts were removed. 5) For the Maker predicted transcripts, expression and size filters were applied to remove transcripts with expression <1 RPKM and size <500 bp. 275 transcripts were removed.

Our final transcriptome is comprised of 14,346 transcripts (84.9% TopHat, 8.4% Maker predictions, 6.1% Oases with match to genome, and 0.6% Oases without match to genome). The total transcriptome size is 34 Mb with average transcript length of 2,354 bp.

RNA-seq for differential gene expression analyses

Tissue was collected and immediately frozen on dry ice in 100 μL Trizol (Life Technologies) before RNA extraction. Tissue homogenization was performed as the mixture was in a semi-frozen state using RNase-free pestles and a pestle motor. RNA was purified using the Direct-zol RNA MiniPrep kit (Zymo). RNA quality was assessed using Bioanalyzer, libraries were

prepared with TruSeq Stranded mRNAseq Sample Prep kit (Illumina), and sequenced on two lanes on a HiSeq2500 chip. We performed paired-end sequencing and obtained ~20 million reads per sample. Samples were obtained in triplicate. To identify irradiation-sensitive genes, 2 mm anterior tapeworm fragments were cut from 10 worms after 3 days *in vitro*. To identify differentially expressed transcripts across the neck A-P axis, 1 mm fragments were cut from 20 freshly obtained 6-day old tapeworms. Differential gene expression analysis was performed using CLC Genomics Workbench (Qiagen) by mapping to our assembled transcriptome (above).

In situ hybridization

WISH and FISH protocols were modified from previously published methods for planarians[36] and the mouse bile-duct tapeworm *Hymenolepis microstoma* (Peter Olson, personal communication). Tapeworms were heat killed and fixed in 4% formaldehyde/10% DMSO/1% NP40/PBSTx for 30 min at room temperature before washing and dehydration into methanol. Dehydrated samples were kept at -30°C for at least 2 days. After rehydration, samples were permeabilized in 10 µg/mL Proteinase-K/0.1% SDS/PBSTx, washed into x 0.1 M Triethanolamine pH7-8 (TEA), 2.5 µL/mL acetic anhydride was added for 5 min with vigorous swirling, acetic anhydride step was repeated, washed in PBSTx and post-fixed in 4% formaldehyde/PBSTx for 10 min. Probe synthesis, hybridization, and staining were performed as previously described[36] using probe concentrations at ~50 ng/mL for 16-48 hrs at 56°C. All probes were synthesized with either DIG or DNP haptens and detected using the following antibodies, all at 1:2000: anti-DIG-AP (Sigma), anti-DIG-POD (Roche), anti-DNP-HRP (Vector Labs). Colorimetric development was done using NBT (Roche)/BCIP (Sigma) or with Fast-Blue (Sigma)[38]. Fluorescent signal was visualized after TSA reaction[36]. DAPI staining and mounting were performed as described above.

418

419 Microscopy

420 Confocal imaging was performed on a Zeiss LSM 880 with the following objectives: 10X
421 PlanNEOFLUOR air, NA 0.3/ 20X Plan-APOCHROMAT air, NA 0.8/ 40X C-APOCHROMAT
422 oil, NA 1.3/ 63X Plan-APOCHROMAT oil, NA 1.4. WISH samples and whole-mount DAPI-
423 stained worms were imaged using a Zeiss AxioZoom V16. Image processing was performed using
424 ImageJ.

425

426 RNAi

427 Double-stranded RNA (dsRNA) was synthesized as previously described[39] and
428 resuspended at concentrations ~ 1.5-2 μg/μL. For control injections, 1.5 kb dsRNA derived from
429 an irrelevant bacterial sequence was used. 6-day old tapeworms were obtained and microinjected
430 with dsRNA using femtotips II via the Femtojet injection system (Eppendorf) to obtain spreading
431 across the first ~ 3-4 mm anterior of the tapeworm. The spread of injected fluids could be detected
432 by a temporary increase in opacity. 500 hPa injection pressure for 0.3-0.8 ms was used per injection
433 site. Whole tapeworms were cultured *in vitro* for 3 days and then 2 mm anterior fragments were
434 amputated and cultured for another 3 days. On day 6, the fragments were re-injected with dsRNA
435 throughout the whole fragment and returned to *in vitro* culture for 9 days before they were
436 terminated for analysis.

437

438 Cell transplantations

439 For dissociated cell preparations, tapeworms were placed in a drop of calcium-magnesium
440 free HBSS (CMF HBSS, Gibco), minced into small pieces with a tungsten needle, incubated in

441 3X Trypsin-EDTA (59418C, Sigma) in CMF HBSS for 20 min at 37°C and dissociated using a
442 dounce homogenizer (Kontes). Cells were pelleted by centrifugation at 250 g for 5 min. The cell
443 pellet was washed in CMF HBSS and passed through cell strainers at 100 μm, 40 μm, 20 μm, and
444 10 μm (Falcon and Sysmex) with one spin and wash in between. Cells were pelleted and
445 resuspended in ~ 200-400 μL WH4 with 0.05% BSA. Cell injections were performed using the
446 Cell Tram Oil 4 injection system (Eppendorf) into the necks of irradiated worms. Injected worms
447 were cultured *in vitro* for 3 days before 5 mm anterior fragments were amputated and grown for
448 an additional 27 days.

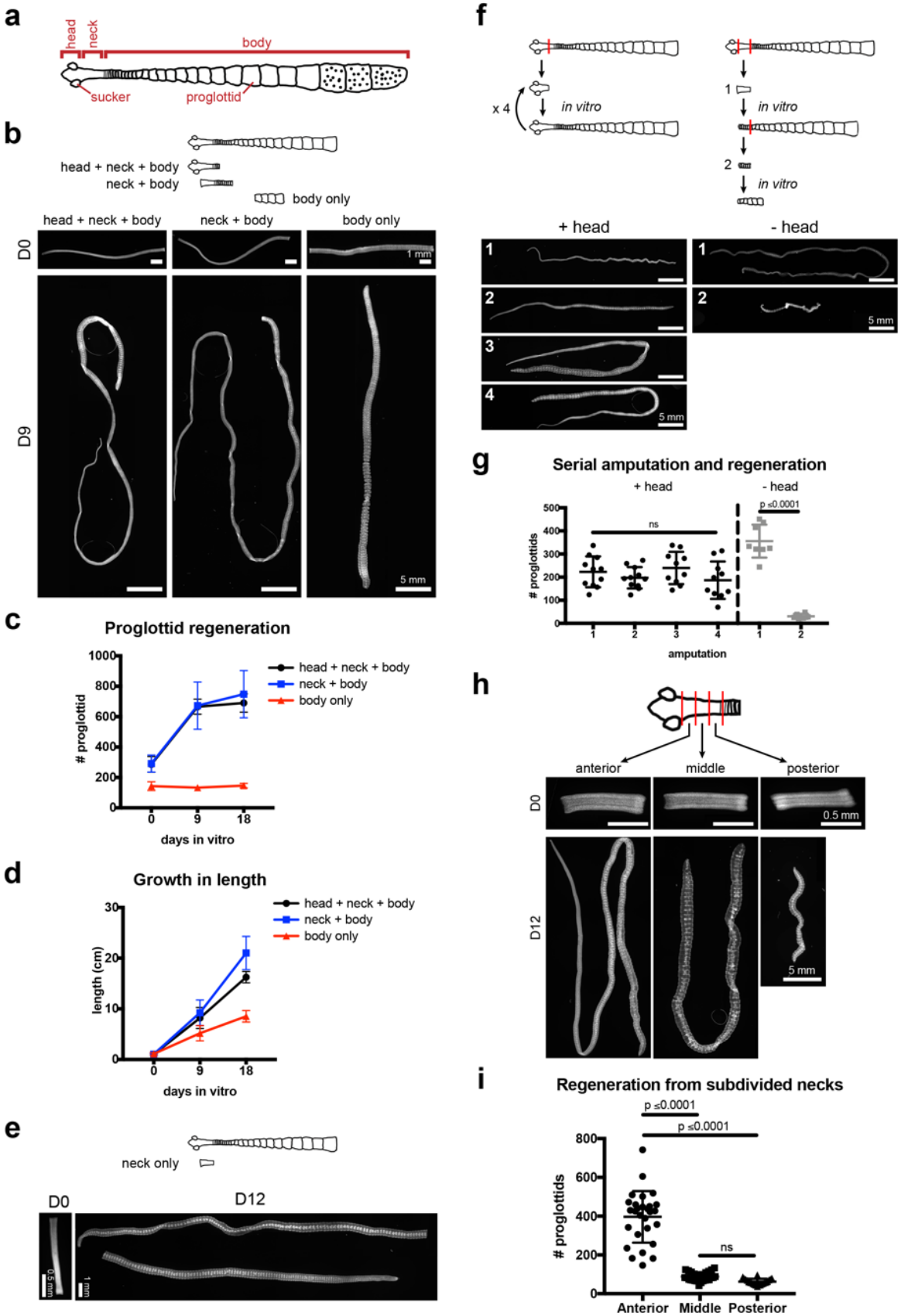

449

Figure 1. Regeneration competence of *H. diminuta*. a, Schematic of *H. diminuta* adults. The tapeworm head includes suckers that attach the worm to the intestine. The neck is defined as the unsegmented region between the head and body. The proglottids grow in an anterior-to-posterior direction and increase in reproductive maturity as they are displaced posteriorly. The most posterior proglottids are gravid with embryos (dotted). We used 6-day old tapeworms that were not yet gravid. **b**, DAPI-stained 1 cm tapeworm fragments before and after 9 days in culture. **c-d**, Quantification of proglottid number and growth in length from (**b**). Error bars=SD, N=2-5, n=7-21 for each timepoint and condition. **e**, Representative DAPI-stained "neck only" fragments before and after 12 days *in vitro*. **f-g**, DAPI-stained fragments after serial amputation. 2 mm anterior fragments, with or without the head, were grown *in vitro* for 12-15 days and then re-amputated serially. Error bars=SD, one-way ANOVA for +head samples, t-test for -head samples. **h-i**, The neck was subdivided into 1 mm fragments from the anterior, middle, and posterior of the neck and grown *in vitro*. DAPI-stained worms are shown. Error bars=SD, N=3, n=22-29 per condition, one-way ANOVA.

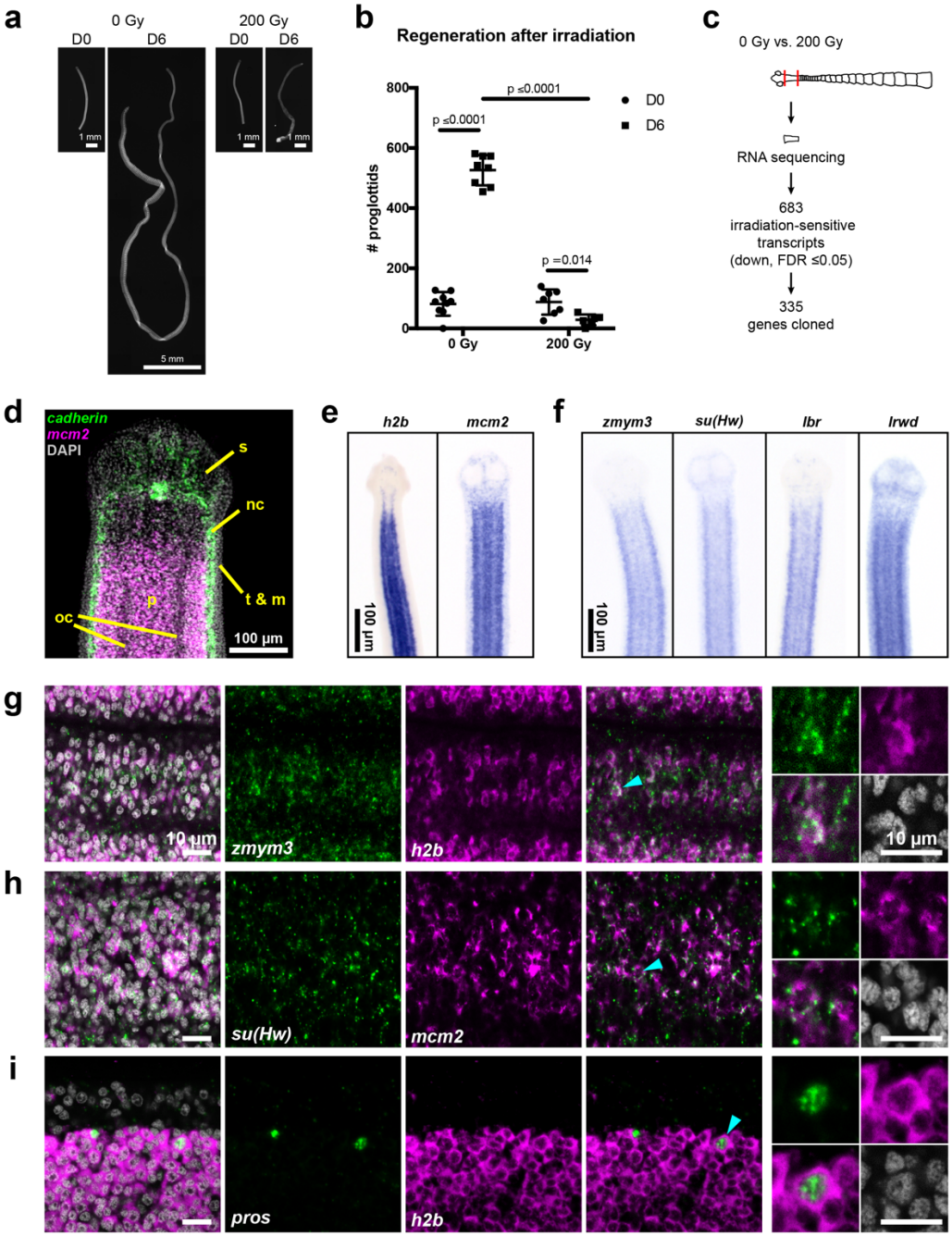

Figure 2. Identification of cycling somatic cell genes using RNA-seq. a-b, DAPI staining of 5 mm anterior fragments from control and irradiated worms before and after *in vitro* culture for 6 days. Error bars=SD, one-way ANOVA. **c**, Schematic of RNA-seq strategy to identify irradiation-sensitive transcripts. **d**, Confocal section of a tapeworm anterior. Cycling cells marked by *mcm2* (magenta) are confined to the neck parenchyma between the nerve cords marked by *cadherin* (green). (s: sucker, nc: nerve cord, oc: osmoregulatory canal, t: tegument, m: muscle, and p: parenchyma). **e**, WISH of known cycling cell markers *h2b* and *mcm2*. **f**, WISH for genes expressed in the neck parenchyma similar to *h2b* and *mcm2*. **g-i**, Confocal sections of dFISH for irradiation-sensitive genes (green) with *h2b* or *mcm2* (magenta). Cyan arrowheads indicate cells that are magnified at the far right.

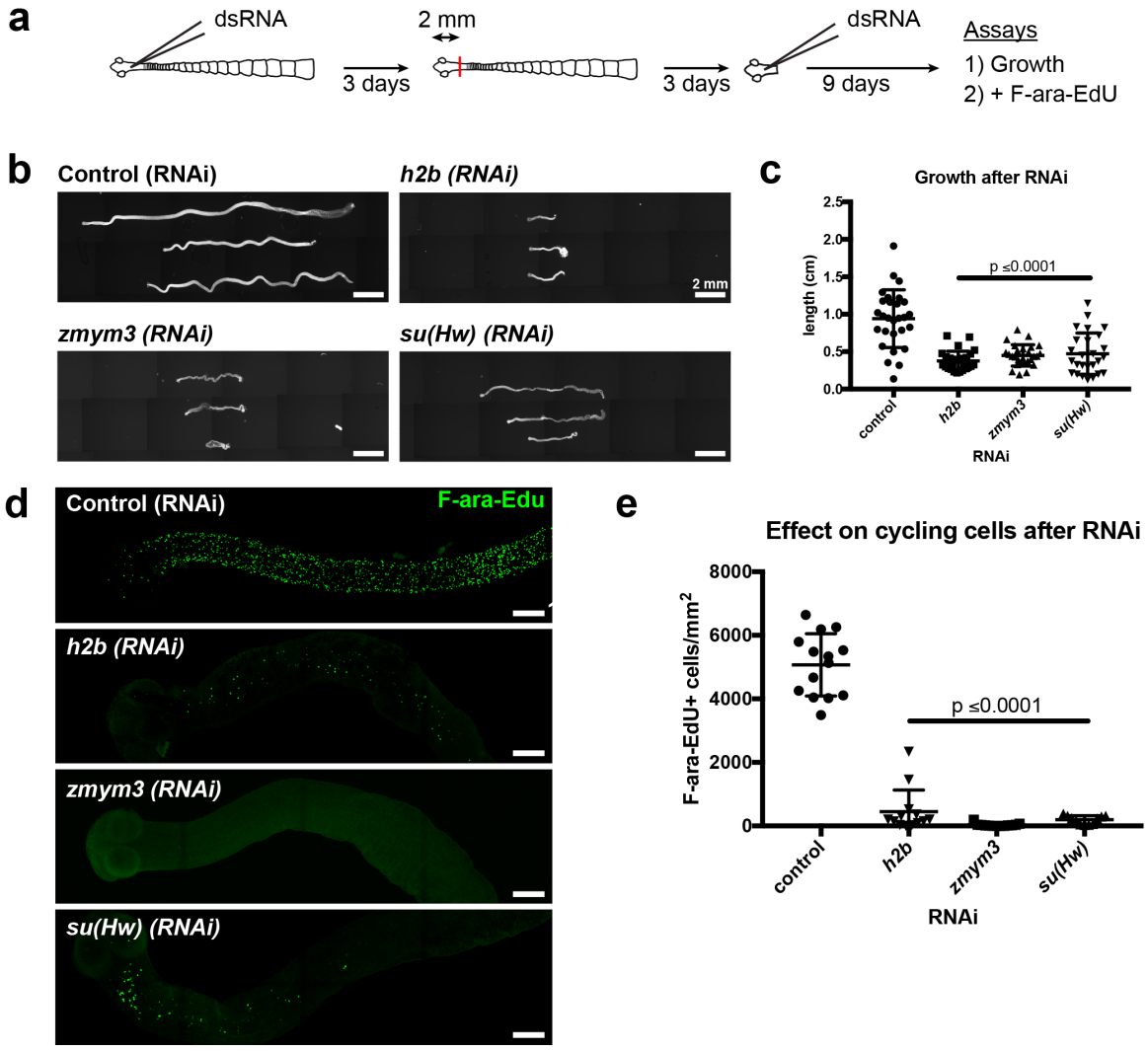

Figure 3. RNAi to identify genes required for proper growth and regeneration in *H. diminuta*. **a**, Schematic of RNAi paradigm. **b**, DAPI-stained worms after RNAi knockdown of *h2b, zmym3*, or *su(Hw)*. **c**, Quantification of worm lengths after RNAi. Error bars=SD, N=3-4, n=26-37, one-way ANOVA. **d**, Maximum-intensity projections from confocal z-stacks at tapeworm necks after RNAi. Panels are oriented anterior facing left. **e**, Quantification of (**d**). Number of F-ara-EdU^{+} cells was normalized to total area from maximum-intensity projection of the DAPI stain. Error bars=SD, N=3, n=11-14, one-way ANOVA.

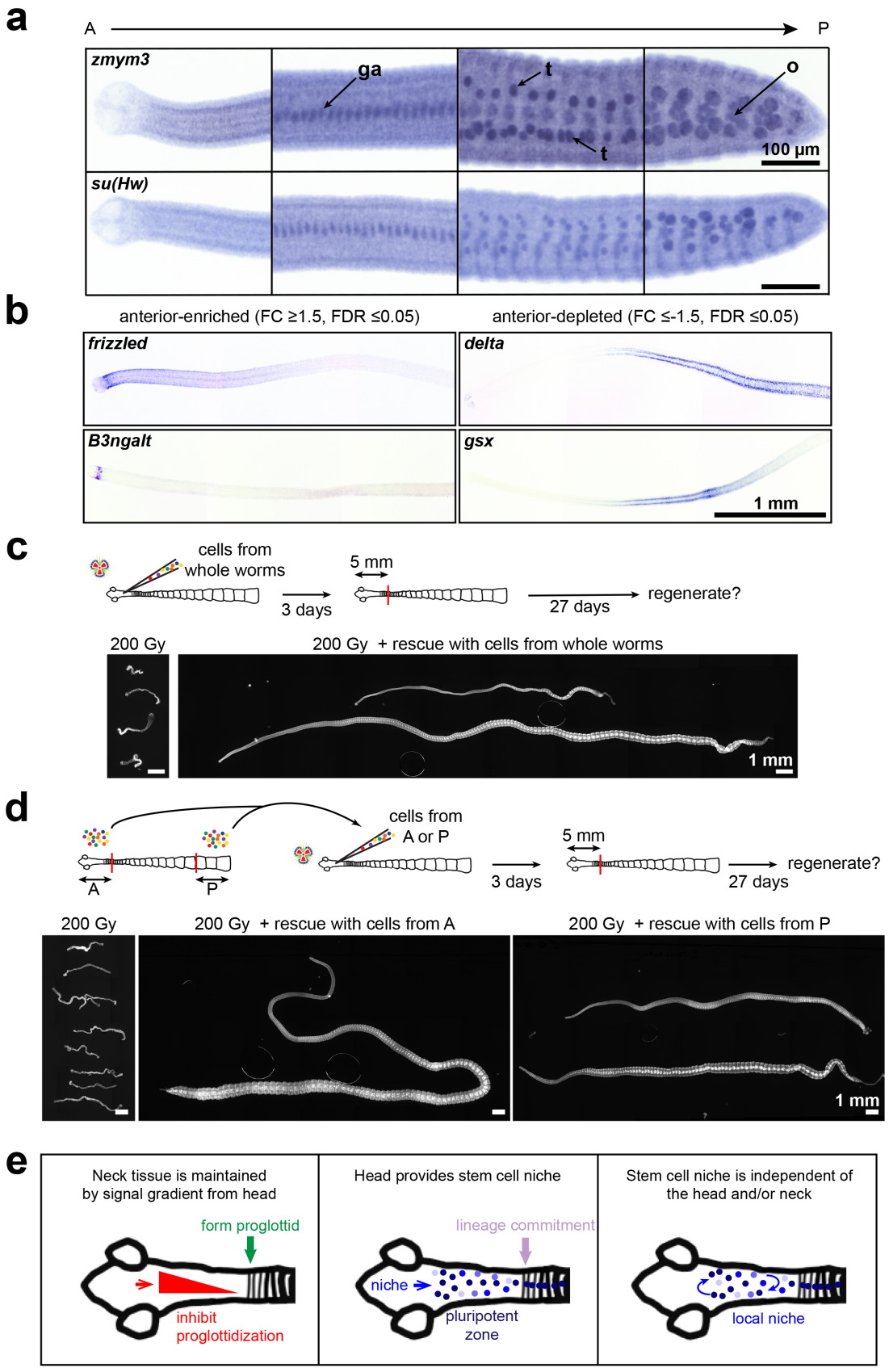

483

Figure 4. Rescue of lethally irradiated tapeworms by cell transplantation. a, WISH patterns for cycling cell genes across the tapeworm A-P axis (ga: genital anlagen; t: testis; o: ovary). **b,** WISH at tapeworm anteriors for genes that were anteriorly enriched or anteriorly depleted by RNA-seq across the A-P axis of the neck only (refer to Fig. 1h). Panels are oriented anterior facing left. **c**, DAPI-stained worms after rescue with cell transplants from whole worms. **d**, DAPI-stained worms after rescue with cell transplants sourced from 5 mm anteriors (A) or 5 mm posteriors (B). **e**, Models for how region-specific regeneration is regulated in *H. diminuta.*

491 **Supplemental Figures**

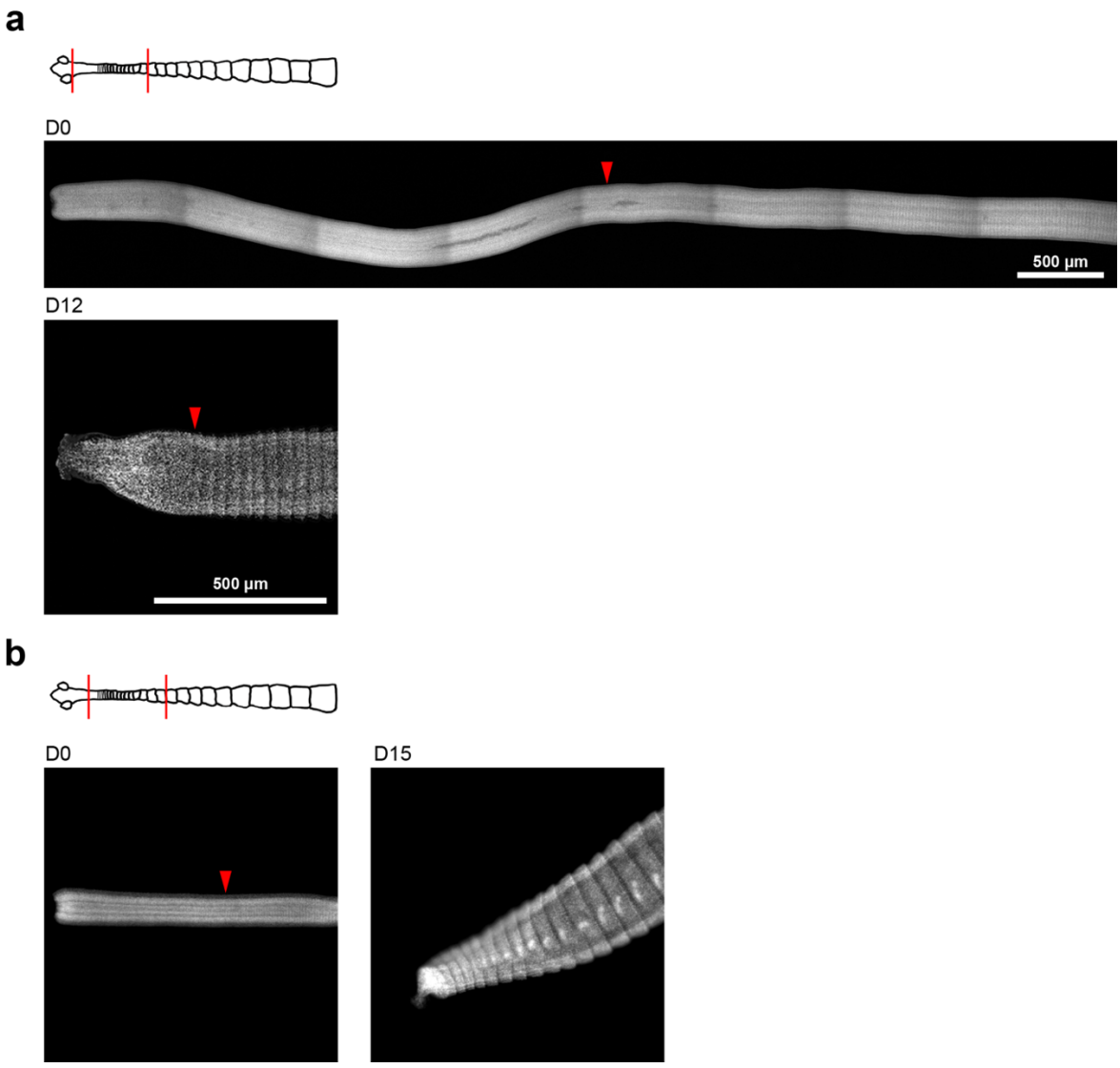

492

493 **Figure S1. Unsegmented neck is depleted after decapitation. a-b**, DAPI-stained worms after
494 decapitation cultured *in vitro* for the indicated number of days. Red arrowheads mark the position
495 of the first visible proglottid. **b**, Worms were amputated 2 mm posterior to the head to remove
496 most of the neck tissue before culturing. After 15 days *in vitro* the neck tissue is no longer
497 identifiable.

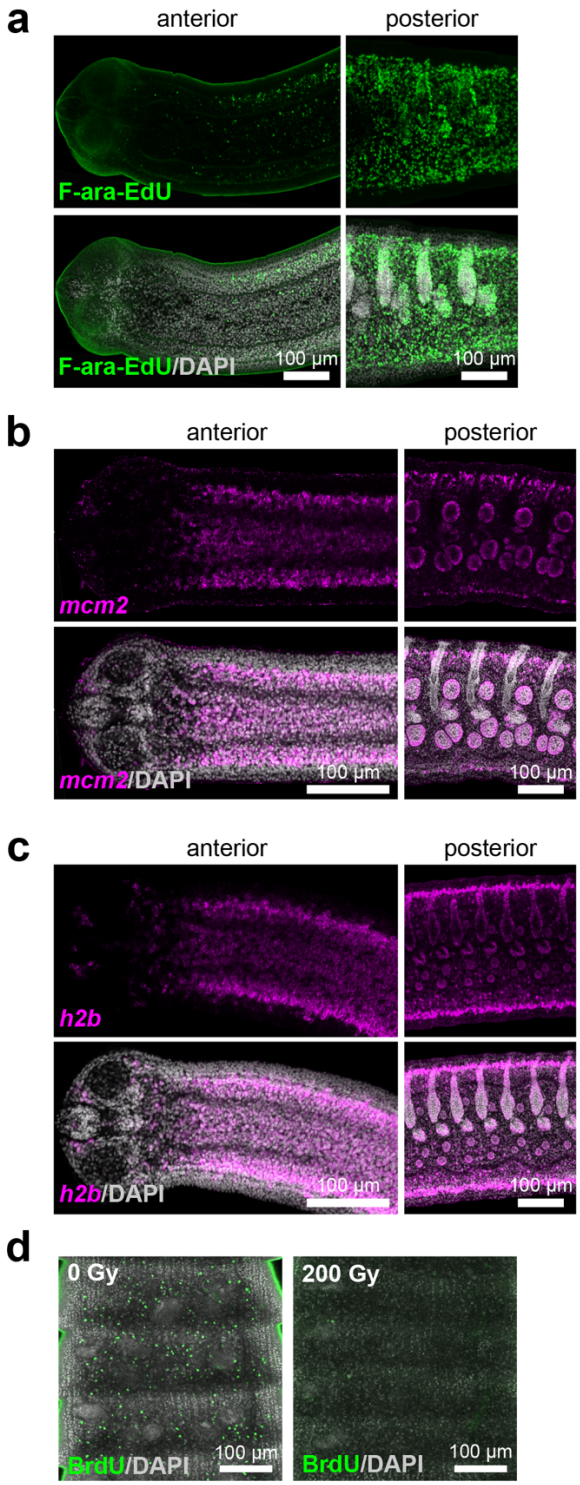

Figure S2. Cycling somatic cells are distributed throughout the whole tapeworm body and are irradiation sensitive. a-c, Confocal sections after uptake of F-ara-Edu for 1 hr (**a**) or FISH to detect *mcm2* (**b**) or *h2b* (**c**). Panels are oriented anterior facing left. **d,** Confocal sections of BrdU labeled tapeworms +/- irradiation. Uptake of BrdU for 1 hr, through a section in the worm body after exposure to 200 Gy irradiation.

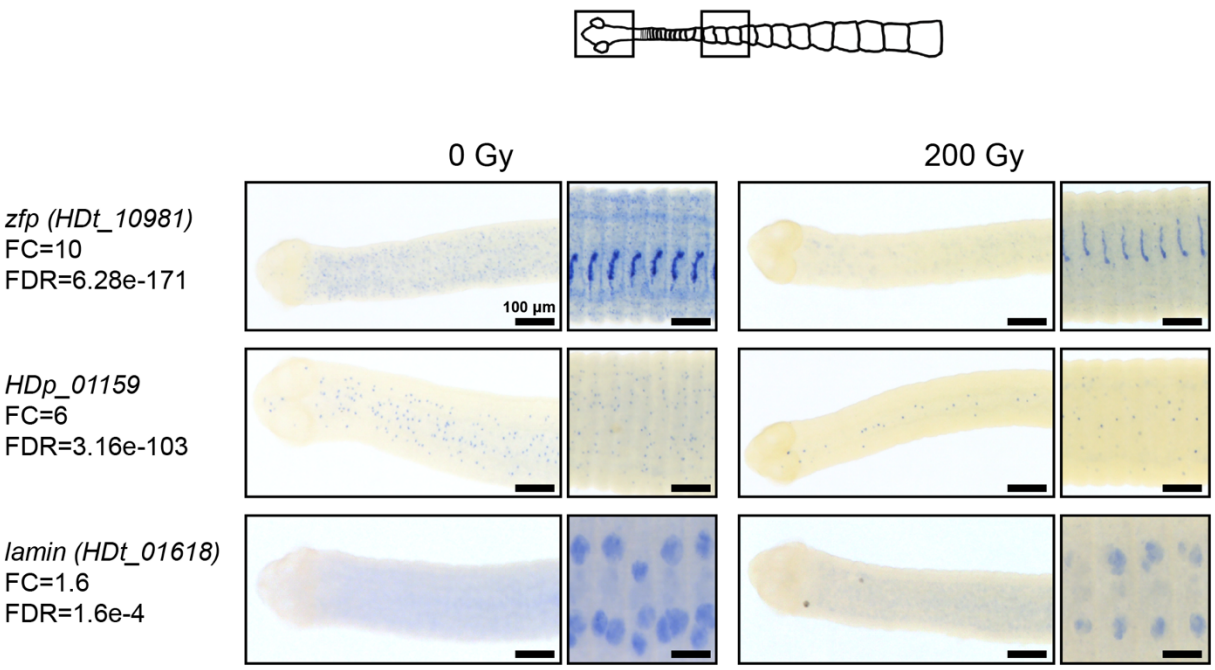

Figure S3. Validation of RNA-seq results by WISH after irradiation. WISH from two regions of the tapeworm: anterior (left) and body (right), +/- exposure to irradiation followed by 3 days *in vitro*.

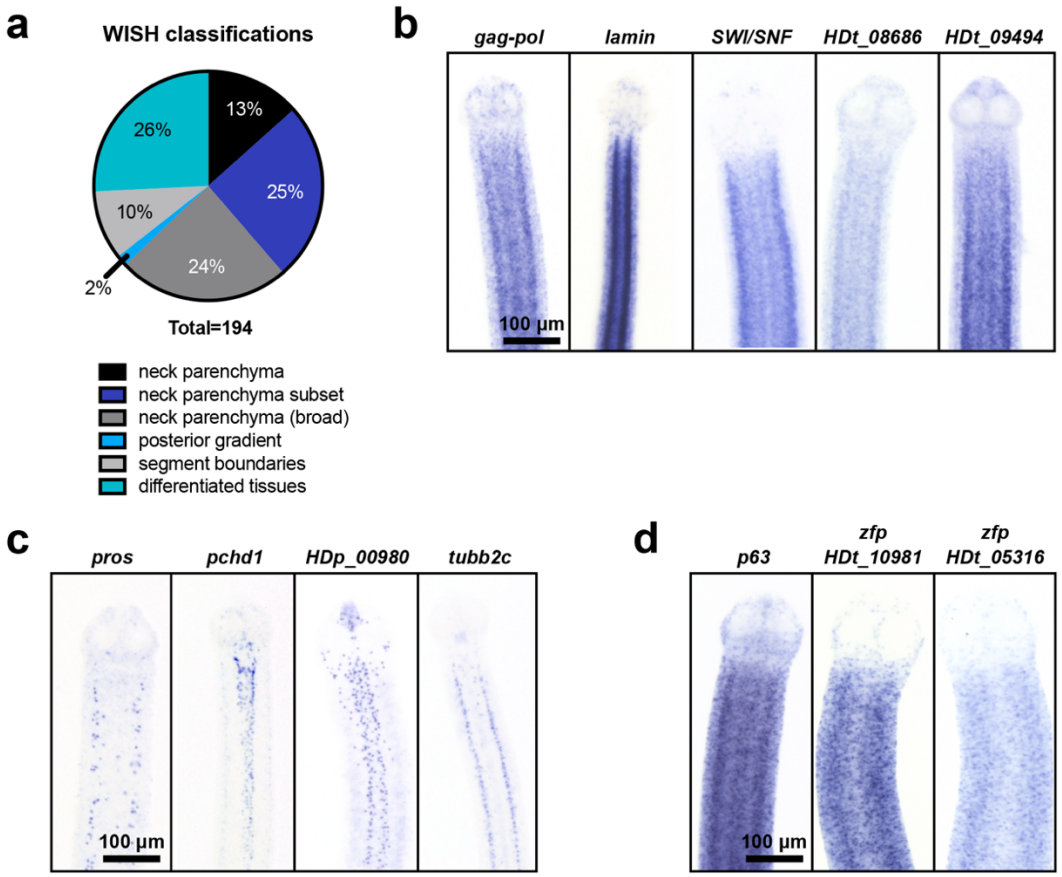

Figure S4. WISH patterns of potential cycling cell genes identified using RNA-seq. a, Classification of WISH expression patterns. **b-d**, WISH patterns at tapeworm necks with anterior oriented up. **b**, Examples of genes expressed in the neck parenchyma. **c**, Examples of genes expressed in a subset of cells within the neck. **d**, Examples of genes expressed broadly in the neck including toward the animal edge where differentiated muscle and tegument are located.

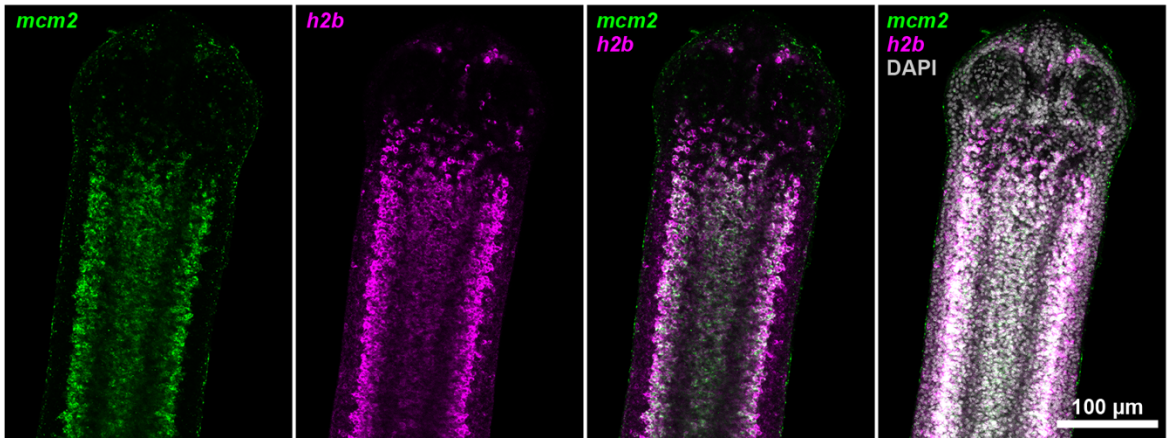

Figure S5. Colocalization of *mcm2* and *h2b.* Confocal section of dFISH to detect *mcm2* (green) and *h2b* (magenta) in the neck parenchyma. Panels are oriented anterior up.

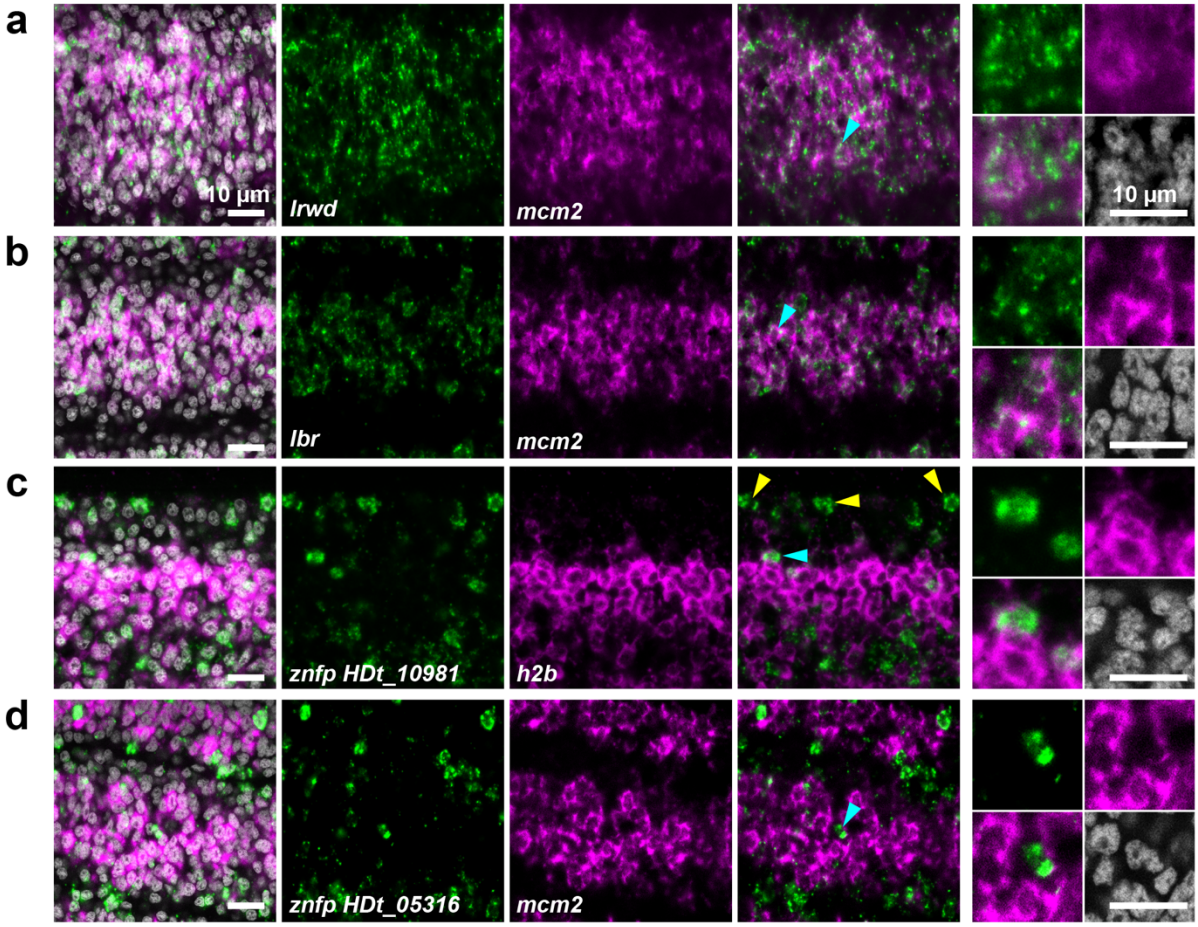

518

519 **Figure S6. The cycling somatic cell population is heterogeneous. a-d**, Confocal sections of
520 dFISH to detect irradiation-sensitive genes (green) with *h2b* or *mcm2* (magenta). Cyan arrowheads
521 indicate cells that are magnified at the far right. Yellow arrowheads point to examples of
522 expression in non-cycling cells. **e**, Summary of different co-expression patterns obtained from 53
523 dFISH experiments.

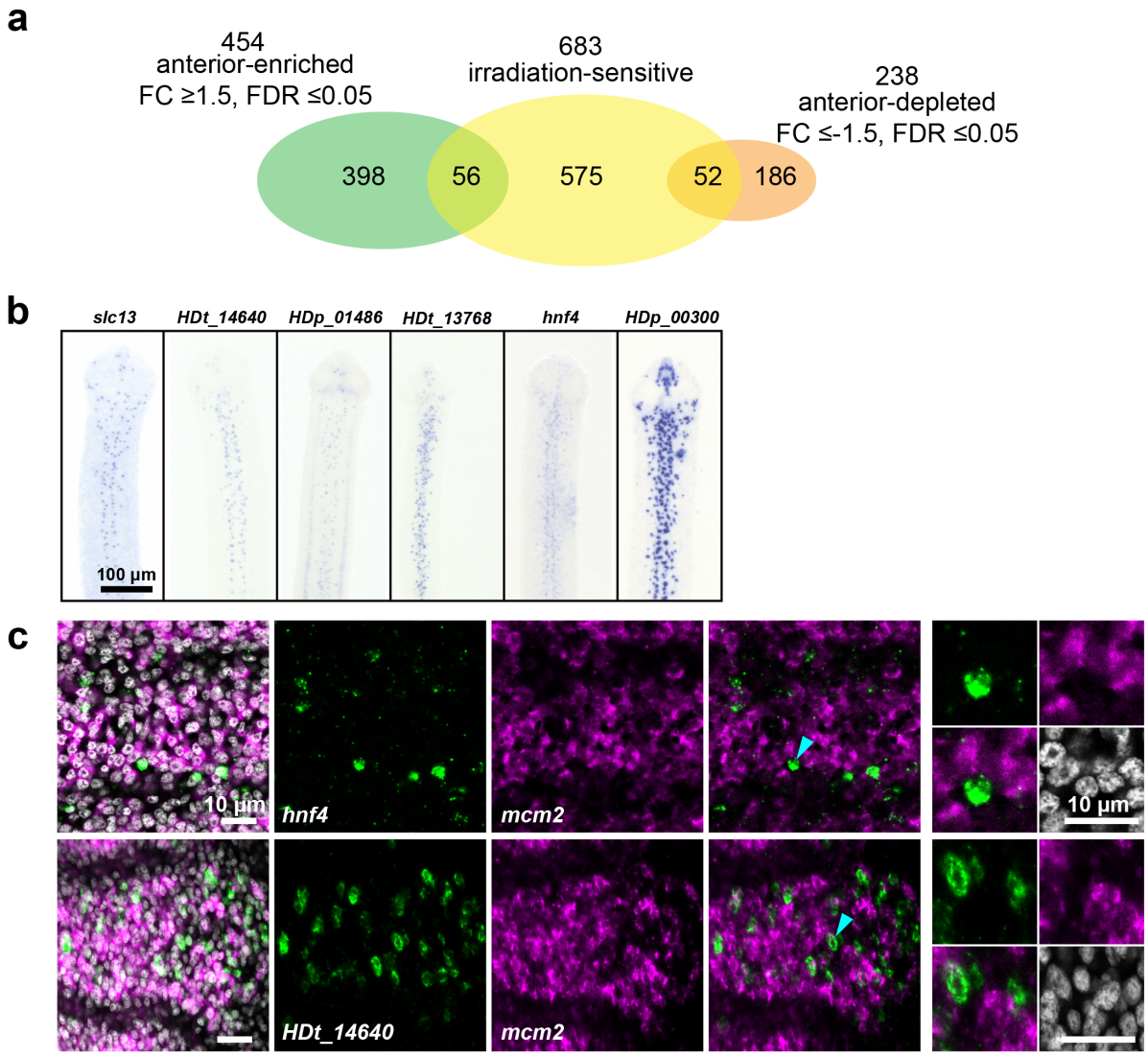

Figure S7. RNA-seq identifies anterior-enriched genes that are expressed predominantly in non-cycling cells. a, Differential gene expression analysis of anterior, middle, and posterior neck fragments from Fig. 1h was used to identify anterior-enriched and anterior-depleted transcripts. Transcripts were considered anteriorly enriched if they were upregulated in the anterior vs. middle or posterior fragments with fold change ≥1.5 and FDR ≤0.05 and conversely for anterior-depleted transcripts. Overlap with irradiation-sensitive transcripts is shown. **b**, WISH of genes that were anteriorly enriched and irradiation sensitive. All panels are oriented with anterior facing up. **c**, Confocal sections of dFISH to detect genes from (**b**), with *mcm2* (magenta). Cyan arrowheads indicate cells that are magnified at the far right.

References

1. Roberts, L. S. The influence of population density on patterns and physiology of growth in *Hymenolepis diminuta* (Cestoda:Cyclophyllidea) in the definitive host. *Exp. Parasitol.* **11,** 332–371 (1961).
2. Del Brutto, O. H. Human cysticercosis (*Taenia solium*). *Trop Parasitol* **3,** 100–103 (2013).
3. Craig, P. & Ito, A. Intestinal cestodes. *Curr. Opin. Infect. Dis.* **20,** 524–532 (2007).
4. Arai, H. P. *Biology of the Tapeworm Hymenolepis diminuta*. (Academic Press, Inc., 1980).
5. Read, C. P. Longevity of the tapeworm, *Hymenolepis diminuta*. *J. Parasitol.* **53,** 1055–1056 (1967).
6. Newmark, P. A. & Sánchez Alvarado, A. Not Your Father's Planarian: A Classic Model Enters The Era Of Functional Genomics. *Nat. Rev. Genet.* **3,** 210–219 (2002).
7. Reddien, P. W. The Cellular and Molecular Basis for Planarian Regeneration. *Cell* **175,** 327–345 (2018).
8. Baguñà, J. The planarian neoblast: the rambling history of its origin and some current black boxes. *Int. J. Dev. Biol.* **56,** 19–37 (2012).
9. Roberts, L. S. Development of *Hymenolepis diminuta* in its definitive host in *Biology of the Tapeworm Hymenolepis Diminuta,* 357–423 (Academic Press, Inc., 1980).
10. Collins, J., III *et al.* Adult somatic stem cells in the human parasite *Schistosoma mansoni*. *Nature* **494,** 476–479 (2013).
11. Koziol, U., Rauschendorfer, T., Zanon Rodríguez, L., Krohne, G. & Brehm, K. The unique stem cell system of the immortal larva of the human parasite *Echinococcus multilocularis*. *EvoDevo* **5,** 10 (2014).
12. Wang, B., Collins, J., III & Newmark, P. A. Functional genomic characterization of neoblast-like stem cells in larval *Schistosoma mansoni*. *eLife* **2,** e00768 (2013).
13. Tsai, I. J. *et al.* The genomes of four tapeworm species reveal adaptations to parasitism. *Nature* **496,** 57–63 (2013).
14. Brehm, K. & Koziol, U. On the importance of targeting parasite stem cells in anti-echinococcosis drug development. *Parasite* **21,** 72 (2014).
15. Goodchild, C. G. Transfaunation and repair of damage in the rat tapeworm, *Hymenolepis diminuta*. *J. Parasitol.* **44,** 345–351 (1958).
16. Schiller, E. L. A simplified method for the in vitro cultivation of the rat tapeworm, *Hymenolepis diminuta*. *J. Parasitol.* **51,** 516–518 (1965).
17. Bolla, R. I. & Roberts, L. S. Developmental physiology of cestodes. IX. Cytological characteristics of the germinative region of *Hymenolepis diminuta*. *J. Parasitol.* **57,** 267–277 (1971).
18. Sulgostowska, T. The development of organ systems in cestodes. I. A study of histology of *Hymenolepis diminuta* (Rudolphi, 1819) (Hymenolepididae). *Acta Parasitologica Polonica* **20,** 449–462 (1972).
19. Solana, J. *et al.* Defining the molecular profile of planarian pluripotent stem cells using a combinatorial RNAseq, RNA interference and irradiation approach. *Genome Biol.* **13,** R19 (2012).
20. Eisenhoffer, G. T., Kang, H. & Sánchez Alvarado, A. Molecular analysis of stem cells and their descendants during cell turnover and regeneration in the planarian *Schmidtea mediterranea*. *Cell Stem Cell* **3,** 327–339 (2008).

21. Koziol, U. & Castillo, E. Cell proliferation and differentiation in cestodes. *Research in Helminths* 121–138 (2011).
22. Collins, J., III, Wendt, G. R., Iyer, H. & Newmark, P. A. Stem cell progeny contribute to the schistosome host-parasite interface. *eLife* **5,** 243 (2016).
23. Pierson, L. *et al.* RNA interference in a cestode reveals specific silencing of selected highly expressed gene transcripts. *Int. J. Parasitol.* **40,** 605–615 (2010).
24. Mizukami, C. *et al.* Gene silencing in *Echinococcus multilocularis* protoscoleces using RNA interference. *Parasitol. Int.* **59,** 647–652 (2010).
25. Spiliotis, M. *et al. Echinococcus multilocularis* primary cells: improved isolation, small-scale cultivation and RNA interference. *Mol. Biochem. Parasitol.* **174,** 83–87 (2010).
26. Pouchkina-Stantcheva, N. N., Cunningham, L. J., Hrčkova, G. & Olson, P. D. RNA-mediated gene suppression and in vitro culture in *Hymenolepis microstoma*. *Int. J. Parasitol.* **43,** 641–646 (2013).
27. Hu, X. *et al.* Gene knockout of *Zmym3* in mice arrests spermatogenesis at meiotic metaphase with defects in spindle assembly checkpoint. *Cell Death Dis* **8,** e2910 (2017).
28. Leung, J. W. C. *et al.* ZMYM3 regulates BRCA1 localization at damaged chromatin to promote DNA repair. *Genes Dev.* **31,** 260–274 (2017).
29. Gdula, D. A., Gerasimova, T. I. & Corces, V. G. Genetic and molecular analysis of the gypsy chromatin insulator of *Drosophila*. *Proc. Natl. Acad. Sci. U.S.A.* **93,** 9378–9383 (1996).
30. Sikes, J. M. & Newmark, P. A. Restoration of anterior regeneration in a planarian with limited regenerative ability. *Nature* **500,** 77–80 (2013).
31. Liu, S. Y. *et al.* Reactivating head regrowth in a regeneration-deficient planarian species. *Nature* **500,** 81–84 (2013).
32. Umesono, Y. *et al.* The molecular logic for planarian regeneration along the anterior-posterior axis. *Nature* **500,** 73–76 (2013).
33. Koziol, U., Jarero, F., Olson, P. D. & Brehm, K. Comparative analysis of Wnt expression identifies a highly conserved developmental transition in flatworms. *BMC Biol.* **14,** 1 (2016).
34. Forsthoefel, D. J. *et al.* An RNAi screen reveals intestinal regulators of branching morphogenesis, differentiation, and stem cell proliferation in planarians. *Dev. Cell* **23,** 691–704 (2012).
35. Collins, J., III, King, R. S., Cogswell, A., Williams, D. L. & Newmark, P. A. An atlas for *Schistosoma mansoni* organs and life-cycle stages using cell type-specific markers and confocal microscopy. *PLoS Negl Trop Dis* **5,** e1009 (2011).
36. King, R. S. & Newmark, P. A. In situ hybridization protocol for enhanced detection of gene expression in the planarian *Schmidtea mediterranea*. *BMC Dev. Biol.* **13,** 8 (2013).
37. Salic, A. & Mitchison, T. J. A chemical method for fast and sensitive detection of DNA synthesis in vivo. *Proceedings of the National Academy of Sciences* **105,** 2415–2420 (2008).
38. Currie, K. W. *et al.* HOX gene complement and expression in the planarian *Schmidtea mediterranea*. *EvoDevo* **7,** 7 (2016).
39. Rouhana, L. *et al.* RNA interference by feeding in vitro-synthesized double-stranded RNA to planarians: methodology and dynamics. *Dev. Dyn.* **242,** 718–730 (2013).